Metastable states in the Ising model with Glauber-Kawasaki competing dynamics

R. A. Dumer [*] and M. Godoy [†]
Instituto de Física–Universidade Federal de Mato Grosso, 78060-900, Cuiabá, Mato Grosso, Brazil

(Received 26 April 2024; accepted 6 August 2024; published 29 August 2024)

Metastable states are identified in the Ising model with competition between the Glauber and Kawasaki dynamics. The model of interaction between magnetic moments was implemented on a network where the degree distribution follows a power law of the form $P(k) \sim k^{-\alpha}$. The evolution toward the stationary state occurred through the competition between two dynamics, driving the system out of equilibrium. In this competition, with probability q, the system was simulated in contact with a heat bath at temperature T by the Glauber dynamics, while with probability $1-q$, the system experienced an external energy influx governed by the Kawasaki dynamics. The phase diagrams of T as a function of q were obtained, which are dependent on the initial state of the system, and exhibit first- and second-order phase transitions. In all diagrams, for intermediate values of T, the phenomenon of self-organization between the ordered phases was observed. In the regions of second-order phase transitions, we obtained the critical exponents of the order parameter β, susceptibility γ, and correlation length ν. Furthermore, in the regions of first-order phase transitions, we have demonstrated the instability due to transitions between ordered phases through hysteresislike curves of the order parameter, in addition to the existence of absorbing states. We also estimated the value of tricritical points when the discontinuity in the order parameter in the phase transitions was no longer observed.

DOI: 10.1103/PhysRevE.110.024315

I. INTRODUCTION

One of the main points of interest when dealing with nonequilibrium systems is the possibility of encountering phase transitions with characteristics of reversible systems, even though in this nonequilibrium thermodynamic regime, we lack a unifying framework like a Gibbs equilibrium statistical mechanics [1]. We can handle systems out of equilibrium when the evolution process toward the steady state involves competition between two dynamics [2–5]. This is because individually these dynamics satisfy detailed balance, but if both have a nonzero probability of acting on the system, the principle of microscopic reversibility is not always respected, and the system is forced out of equilibrium. Two dynamics that are commonly employed in competition are the Glauber dynamics with the single-spin flip process [6] and the Kawasaki dynamics with the two-spin exchange process [7].

Given its simplicity and usefulness in studying phase transitions, the Ising model is also widely employed in investigating nonequilibrium systems with competitive dynamics. In such cases, considering a ferromagnetic coupling between spins, with probability q, the system is in contact with a thermal reservoir at temperature T and relaxes to the steady state of lower energy through the Glauber dynamics. However, with probability $1-q$, the system is subject to an external energy influx and evolves to the state of higher energy through the Kawasaki dynamics. In a regular square lattice [8], the Ising model subject to these competing dynamics self-organizes into the ordered phases, the ferromagnetic phase (F) and the antiferromagnetic phase (AF). In this self-organization, at low values of q, the AF phase is found, corresponding to the higher energy state of the system. But as q increases, a transition occurs to the paramagnetic phase (P). Further increasing q leads to another transition to an ordered phase, the F phase, corresponding to the lower energy state of the system. In this case, the continuous phase transitions were found between the AF to P and P to F phases, except for $q \leqslant 0.2$, where a tricritical point is present, and the first-order phase transitions are observed from the F phase to P.

Beyond regular networks, complex networks despite not having much evidence to describe crystals are of great interest because they describe a range of structures found in society. Examples of these are the small-world networks [9,10], which encompass the property discovered by Milgram [11], wherein any person in the world can have contact with another, requiring a remarkably smaller number of intermediaries compared to the size of the network. Another example of complex networks present in society are those that follow a power-law degree distribution, $p(k) \sim k^{-\alpha}$ [12]. In this case, $p(k)$ is the probability of any point in the network having k other points connected to it, and α is the exponent that depends on the object of study. Networks of this kind stand out because, with advances in data processing techniques and equipment, it has been observed that networks such as the world wide web, the internet, citation networks, networks of actors who have appeared in the same film, networks of protein interactions, among many others [13], despite having very distinct formation origins, self-organize in such a way that the degree distribution takes the form of a power law.

Due to the importance of complex networks, they have been implemented in physical models to investigate their influence on phase transitions [14–17]. These models also

[*]Contact author: rafaeldumer@fisica.ufmt.br
[†]Contact author: mgodoy@fisica.ufmt.br

include the nonequilibrium Ising model through competitive dynamics. With one- and two-spin flips competing dynamics on small-world networks [18] and networks with power-law degree distribution [19], the phenomenon of self-organization is observed. This involves transitions from the AF to P phases and from the P to F phases, varying the competition parameter q. In both cases, only second-order phase transitions are found, and the universality class obtained through critical exponents, in both networks, with and without [20,21] competitive dynamics, belongs to the mean-field regime. The results are also available regarding the Ising model on a 2D small-world network and with competition between the Glauber and Kawasaki dynamics [22]. In this case, the self-organization was also observed, but in the region of phase diagrams ($T \times q$), where competition between the F and AF ordered phases is present, i.e., low values of q and T, first-order phase transitions are found, in addition to second-order phase transitions for low values of q with high values of T, and high values of q with low values of T.

In these studies, both on regular [2,8] and complex networks [22], of the Ising model with competing Glauber and Kawasaki dynamics, first-order phase transitions are found. However, the metastability achieved by applying competing dynamics can alter the topology of phase diagrams given the regions of instability, and depending on the shape of these regions, absorbing states can be identified, but these aspects have not been addressed in previous works. Therefore, we will search for the existence of absorbing states and study the topology of the phase diagrams by altering the initial conditions of the system. Additionally, we intend to make a direct comparison between the nonconservative one- and two-spin flip dynamics applied in previous works [19] and the competition between Glauber and Kawasaki dynamics. To achieve this, we will investigate the Ising model on a network with a power-law degree distribution and with competition between the Glauber and Kawasaki dynamics. In this configuration, each point of the network represents a spin variable that can take values of $\sigma \pm 1$, with a probability $p(k) \sim k^{-1}$ of interacting with k other spins randomly distributed in the network. For the evolution toward the steady state, with probability q, the system is in contact with a thermal reservoir at temperature T and it relaxes to the lowest energy state through Glauber dynamics. Meanwhile, with a probability $1 - q$, there is an external energy flux into the system, governed by Kawasaki dynamics, favoring the higher energy state.

This article is organized as follows: In Sec. II, we present the network, the dynamics involved in the system, and how they drive the evolution of the Ising system. In Sec. III, we provide details about the Monte Carlo method, the thermodynamic quantities of interest, and the scaling relations for each of them. The phase diagrams and a detailed description of both first- and second-order phase transitions present in these diagrams are discussed in Sec. IV. Finally, in Sec. V, we present the conclusions drawn from the study.

II. MODEL

Here, we have utilized a network divided into two sublattices. The sites from one sublattice can only randomly connect to spins of the other sublattice, and the degree of the sites

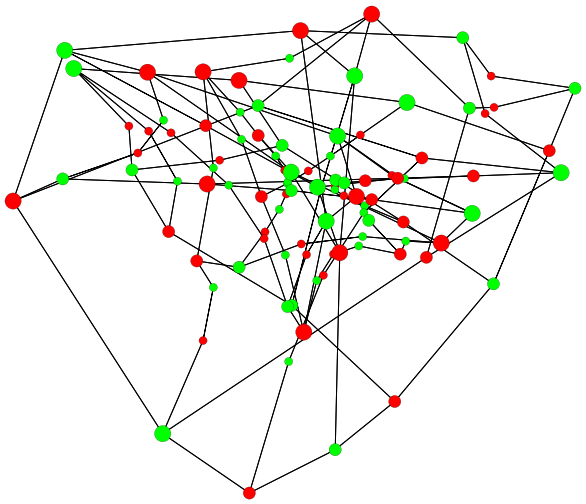

FIG. 1. Representation schematic of the network with a power-law degree distribution, with exponent $\alpha = 1$, $k_m = 4$, $k_0 = 2$, and size $N = (10)^2$. The green (light gray) circles represent one of the sublattices, while the red (dark gray) circles represent the other sublattice. The black lines indicate the connections between the sublattices. The size of the circles corresponds to the degree of the vertex in the network.

follows a power-law distribution of the form

$$p(k) = \frac{k^{-\alpha}}{\sum_{k=k_0}^{k_m} k^{-\alpha}}. \tag{1}$$

With $k_0 = 4$ being the minimum degree of the sites, $k_m = 10$ the maximum degree present on the network, and a fixed value of $\alpha = 1$, we impose limitations on the degrees of the network, thereby disrupting the scale-free network property typically found in real networks exhibiting growth and preferential connections [12]. An example of the network can be seen in Fig. 1, indicating the connection between the two sublattices and the limitation in the network degrees. These choices are made to ensure finite critical points and to verify whether the universality class obtained for the model in the thermodynamic equilibrium regime will prevail in this nonequilibrium system. Therefore, our focus in this study is on the effects of reactive-diffusive competing dynamics on the well-defined network implemented in the Ising model. Further details on the network construction and the effect of the exponent α at the criticality of the system can be found in two previous works [19,21].

In the Ising model, the interaction energy between the spins is defined by the Hamiltonian in the form

$$\mathcal{H} = -\sum_{\langle i,j \rangle} J_{ij}\sigma_i\sigma_j, \tag{2}$$

where $\sigma_i = \pm 1$, the sum is over all pair of spins, and we use $J_{ij} = 1$, meaning ferromagnetic interaction if sites i and j interact between the sublattices, and zero otherwise.

For our nonequilibrium system, let us denote $p(\{\sigma\}, t)$ as the probability of finding the system in the state $\{\sigma\} = \{\sigma_1, \ldots, \sigma_i, \ldots, \sigma_j, \ldots \sigma_N\}$ at time t. The equation governing the evolution of the probability of states over time is given by

the master equation

$$\frac{d}{dt}p(\{\sigma\},t) = qG + (1-q)K, \tag{3}$$

where qG represents the one-spin flip process, associated with the Glauber dynamics, which relaxes the spins in contact with a heat bath at temperature T, favoring the lowest energy state of the system, and have probability q to occur. However, $(1-q)K$ represents the two-spin exchange process, related with the Kawasaki dynamics, where the system is subjected to an external flux of energy into it, increasing the energy of the system, and have probability $1-q$ to occur. G and K are described as follows:

$$G = \sum_{i,\{\sigma'\}}[W(\sigma_i \to \sigma_i')p(\{\sigma\},t) - W(\sigma_i' \to \sigma_i)p(\{\sigma'\},t)], \tag{4}$$

$$K = \sum_{i,j,\{\sigma'\}}[W(\sigma_i\sigma_j \to \sigma_j\sigma_i)p(\{\sigma\},t) - W(\sigma_j\sigma_i \to \sigma_i\sigma_j)p(\{\sigma'\},t)], \tag{5}$$

where $\{\sigma'\}$ is the new the spin configuration, $W(\sigma_i \to \sigma_i')$ is the transition rate between the states on the one-spin flip process, and $W(\sigma_i\sigma_j \to \sigma_j\sigma_i)$ the transition rate between the states in the two-spin exchange process.

III. MONTE CARLO SIMULATIONS

In our Monte Carlo simulations, we have considered two possible initial states for the system: the ordered state, where all the spins are the same state, and the disordered state, where the spin states are randomly chosen. Starting from the initial state, a new spin configuration is generated following the Markov process: for a given temperature T, competition probability q, and network size N, we randomly select a spin σ_i in the network and generate a random number r, uniform distributed between zero and one. If $r \leqslant q$, then we choose the one-spin flip process, in which the flipping probability is given by the Metropolis prescription:

$$W(\sigma_i \to \sigma_i') = \begin{cases} e^{(-\Delta E_i/k_BT)} & \text{if } \Delta E_i > 0, \\ 1 & \text{if } \Delta E_i \leqslant 0, \end{cases} \tag{6}$$

where ΔE_i is the change in energy, based in Eq. (2), after flipping the spin σ_i, k_B is the Boltzmann constant, and T the temperature of the system. In summary, a new state is accepted if $\Delta E_i \leqslant 0$. However, if $\Delta E > 0$, then the acceptance is determined by the probability $\exp(-\Delta E_i/k_BT)$, and it is accepted only if a randomly chosen number r_1 uniformly distributed between zero and one satisfies $r_1 \leqslant \exp(-\Delta E_i/k_BT)$. If none of these conditions are satisfied, then the state of the system remains unchanged. Now, if $r > q$, then the two-spin exchange process is chosen, and in addition to the spin σ_i we also randomly choose one of its neighbors σ_j, and the state of these two spins are exchanged according to transition rate

$$W(\sigma_i\sigma_j \to \sigma_j\sigma_i) = \begin{cases} 0 & \text{if } \Delta E_{ij} \leqslant 0, \\ 1 & \text{if } \Delta E_{ij} > 0, \end{cases} \tag{7}$$

where ΔE_{ij} is the change in the energy after exchange the state of the spins σ_i and σ_j. In this process, the new state is accepted only if the change in energy is positive. This approach simulates the system with an external energy input, where an increase in energy is anticipated.

Repeating the Markov process N times, we have one Monte Carlo step (MCS). We allowed the system to evolve for 10^4 MCS to reach a stationary state, for all network sizes, $(32)^2 \leqslant N \leqslant (256)^2$. To calculate the thermal averages of the quantities of interest, we conducted an additional 4×10^4 MCS, and the averages over the samples were done using 10 independent samples of the initial state of the system. The statistical errors were calculated using the Bootstrap method, which means they were estimated from random samplings of the total number of MCS in the stationary state.

The measured thermodynamic quantities in our simulations are: magnetization per spin m_N^F, staggered magnetization per spin m_N^{AF}, magnetic susceptibility χ_N, and reduced fourth-order Binder cumulant U_N:

$$m_N^F = \frac{1}{N}\left[\left\langle\sum_{i=1}^{N}\sigma_i\right\rangle\right], \tag{8}$$

$$m_N^{AF} = \frac{1}{N}\left[\left\langle\sum_{i=1}^{N}(-1)^{(l+c)}\sigma_i\right\rangle\right], \tag{9}$$

$$\chi_N = \frac{N}{k_BT}[\langle m^2\rangle - \langle m\rangle^2], \tag{10}$$

$$U_N = 1 - \frac{[\langle m^4\rangle]}{3[\langle m^2\rangle^2]}, \tag{11}$$

where $[\ldots]$ representing the average over the samples, and $\langle\ldots\rangle$ the thermal average over the MCS in the stationary state. To facilitate the calculation of m_N^{AF}, the sites on the network are labeled as if we had a square lattice, $N = L^2$, in this way, l and c are the row and column of the site i, respectively. In Eqs. (10) and (11), m can represent either m_N^F or m_N^{AF}.

Near the stationary critical point Γ_c, Eqs. (8), (9), (10), and (11) obey the following finite-size scaling relations [23]:

$$m_N = N^{-\beta/\nu}m_0(N^{1/\nu}\epsilon), \tag{12}$$

$$\chi_N = N^{\gamma/\nu}\chi_0(N^{1/\nu}\epsilon), \tag{13}$$

$$U_N' = N^{1/\nu}\frac{U_0'(N^{1/\nu}\epsilon)}{\Gamma_c}, \tag{14}$$

where $\epsilon = (\Gamma - \Gamma_c)/\Gamma_c$ (Γ can be T or q), β, γ and ν are the critical exponents related the magnetization, susceptibility and correlation length, respectively. The functions $m_0(N^{1/\nu}\epsilon)$, $\chi_0(N^{1/\nu}\epsilon)$ and $U_0(N^{1/\nu}\epsilon)$ are the scaling functions.

IV. RESULTS

This section is divided into four subsections. Sections IV A and IV B are related to the conditional phase diagrams obtained for the system with two different initial states, and the complete phase diagram of the system, containing all the points obtained from these conditional diagrams. Sections IV C and IV D concern the different phase transition types found in the phase diagrams, namely, second- and first-order phase transitions, respectively.

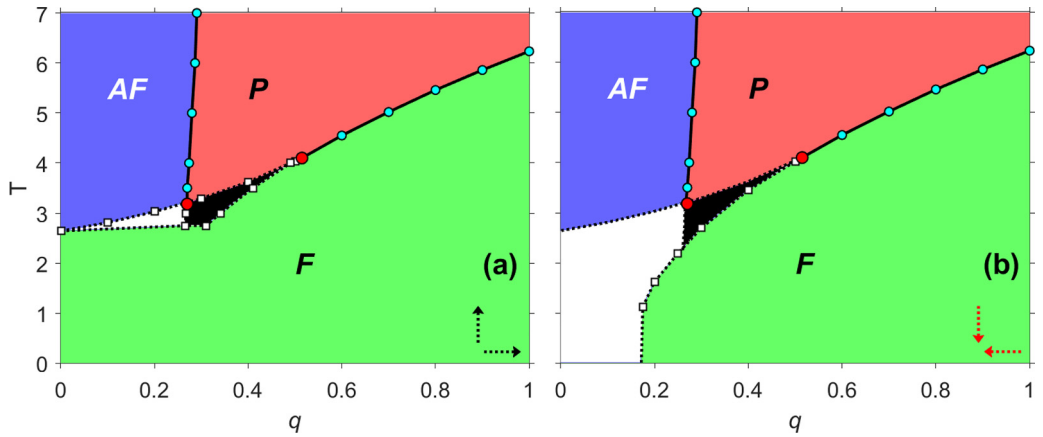

FIG. 2. Conditional phase diagrams $q \times T$ for the ordered initial state of spins in the simulations. These diagrams present regions with different colors and denote the stable phases, AF (purple in the upper left corner), F (green at the bottom), P (red in the upper right corner), and the metastable phases, AF or F (white), F or P (black). The cyan (light gray) circles indicate second-order phase transition points and the white squares indicate first-order phase transition points. The red (dark gray) points represent the tricritical points, and the dashed arrows indicate the direction of sweeping of the parameters T and q in the simulations. The dotted and straight lines are only guides for the eyes, and the error bars are smaller than the symbol sizes.

A. Ordered initial state

In this subsection, the conditional phase diagrams of the system were obtained with the ordered F initial state in the simulations. In the diagram of Fig. 2(a), the phase transition points were found by varying the external parameters, T or q, from the lowest to the highest value (black dashed arrows in the figure). At high values of q and varying T, we have observed a second-order phase transition between the F and P phases. Thus, regardless of the initial state of the system and the starting point of the simulation, we consistently obtained the same critical point value. For temperatures $T \gtrsim 3.18$ and up to $T = 6.235$, we have observed the self-organization phenomena in the system, where we start from the AF phase, at low values of q, and pass to the disordered P phase when reducing the external energy flow into the system. However, we found another ordered phase, the F phase, when the prevailing dynamics involve the system being in contact with a heat bath, at high values of q. A characteristic of the critical points at high temperatures is that they indicate a second-order phase transition. However, at low values of q and T, the first-order phase transitions are found. Regarding these first-order phase transitions, the white-colored region in the diagram indicates that we can have both the F and AF phases in this region, depending on the starting point of the simulations. If we start the simulation with parameter values in the purple region, then we find the AF phase in the white region. Conversely, if we start the simulations with the parameter values in the white region, then we only find the F phase. The black region of the diagram indicates that we can have both the P and F phases in this region, depending on the initial parameter values of the simulations. If we start the simulations with parameter values in the purple region, then we find the P phase in the black region. Nevertheless, if we initiated the simulations with parameter values in the white region, then we have found only the F phase in the black region.

The existence of these phases can be explained by the dynamics implemented in the system. At low values of q, the Kawasaki dynamics prevail in the system, simulating an external energy flow into the system. In this dynamics, the order parameter is conserved, so if we have an initial state with all spins up, as is the case of the diagram in Fig. 2(a) at $q = 0$, the only possible state is the F state. However, if $q \neq 0$, then the system is also influenced by the dynamics simulating the system in contact with a heat bath at temperature T, so at low temperatures, the F phase is expected. Now, when the temperature increases, for low values of q, the Kawasaki dynamics that prevail in the system organize it into the AF phase, the phase of higher energy of the system, as expected, because the dynamics governed by the Metropolis mechanism altered the spin states, so it is possible to find a state different from F. Thus, for high values of T and q, when the dynamics simulating a system in constant contact with a heat bath prevails in the system, the P phase is found. Additionally, characterizing the first-order phase transitions, the white and black regions in the diagram indicate the instability of these states near the critical point and can be further identified in the results throughout this work.

The diagram in Fig. 2(b) was also obtained with the ordered F initial state in the simulations, but the points in this diagram were found by varying the values of the external parameters, T or q, from the highest to lowest (red dashed arrows in the figure). In this case, the second-order phase transition points are the same as those in the diagram in Fig. 2(a), but the way we varied the external parameters allows us to observe new regions due to first-order phase transitions. Similar to the diagram in Fig. 2(a), the white region indicates both the AF and F phases, depending on the parameter values at the beginning of the simulation. If we start the simulation with the parameter q value in the purple region and decrease T, then we always find the AF phase, but if we start the simulation with the T value in the white region, we only find the F phase. The black region indicates both the P and F phases, depending on the parameter values at the beginning of the simulation. If we start the simulation with the parameter

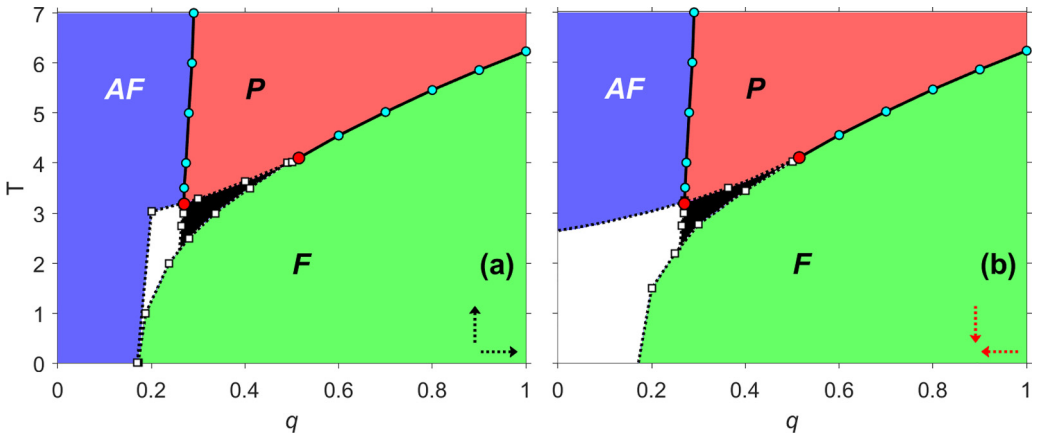

FIG. 3. Conditional phase diagrams $q \times T$ for the random initial state of spins in the simulations. These diagrams present regions with different colors and denote the stable phases, AF (purple on the left side), F (green in the lower right corner), P (red in the upper right corner), and the metastable phases, AF or F (white), F or P (black). The cyan (light gray) circles indicate second-order phase transition points and the white squares indicate first-order phase transition points. The red (dark gray) points represent the tricritical points, and the dashed arrows indicate the direction of sweeping of the parameters T and q in the simulations. The dotted and straight lines are only guides for the eyes, and the error bars are smaller than the symbol sizes.

values in the red region, then the black region represents the P phase. However, if we start the simulation with external parameter values from the black region, then we only find the F phase. The white and black regions were delimited by the points from the diagram in Fig. 2(a), since we could not find transitions from the AF phase to the P phase and from the P phase to the F phase in this diagram. The first-order phase transition points present in the diagram in Fig. 2(b) were obtained by fixing T and varying q, or fixing q and varying T starting from the purple or red region.

The different regions of the diagram in Fig. 2(b), when compared to Fig. 2(a), result of the dynamics involved, as well as the values of the parameters that start the simulation and how they are changed. At low values of q and high values of T, if $q \neq 0$, then the influence of the heat bath on the system is sufficient to change randomly the spin states. Nonetheless, since the prevailing dynamics in the system force it toward the state of higher energy, we can still find the ordered state of the AF phase. Maintaining low values of q and starting from high values of T, when we decrease the temperature in the system, the influence of the dynamics simulating the heat bath in the system is insufficient to obtain an F phase, and only the AF phase is observed. However, at low values of q and starting from T values in the white-colored region, the temperature in the system is not high enough to have disordered spins, so the Glauber mechanism keeps the system ordered.

B. Disordered initial state

In the conditional phase diagrams of Figs. 3(a) and 3(b), we have the steady states obtained for the system with the random spin initial state (disordered initial state) in the simulations. In Fig. 3(a), the variation of the external parameters, T or q, occurs from the lowest to the highest value (black dashed arrows in the figure). When, we have a high external energy flow into the system, i.e., low values of q, only the ordered AF state is found in the system. Yet, when we increase q, the first-order phase transitions from the AF to the F phases are observed. In this diagram, the white-colored region indicates both the AF and F phases, depending on the value of the external parameter from which we start the simulation. If the value of parameter T starts as one of the values in the green region, then the white region represents the F phase. However, if the initial temperature of the system lies between the values of the white region, then only the AF phase is found in this region. The black region in the diagram of Fig. 3(a) can indicate both F and P phases. Starting the simulation with parameter values in the green region, the black region represents the F phase. Now, if the parameter values are in the white or purple region, then the phase found in the black region is the P phase. Additionally, in this diagram, the second-order phase transition points are the same as those found in the diagrams of Figs. 2(a) and 2(b).

The white and black regions in Fig. 3(a) can be interpreted as a metastable state due to the first-order phase transitions in this part of the diagram, where we have a greater influence of the diffusive dynamics, which conserves the order parameter, the Kawasaki dynamics. In this figure, the initial state is one where the spin states are randomly distributed on the lattice sites. At low values of q, the high energy flow into the system ensures that we always have obtained the state of higher energy, given the Hamiltonian of the Ising model. However, when the energy flow decreases, increasing q, the dynamics favoring the lower energy state prevail in the competition between dynamics, and we begin to find the F state in the system at low values of T.

Finally, in the diagram in Fig. 3(b), we also used the disordered initial state of the spins in the simulation, but now the sweeping of the external parameters occurs from the highest to lowest values (red dashed arrows in the figure). In this diagram, there is also a region where both the AF and F phases can coexist, represented by the white-colored region. When fixing q and varying T, we only observed the AF phase in this region. However, when fixing T and varying q and starting from values in the green region, only the F phase is observed. The black region in this diagram also indicates both the P

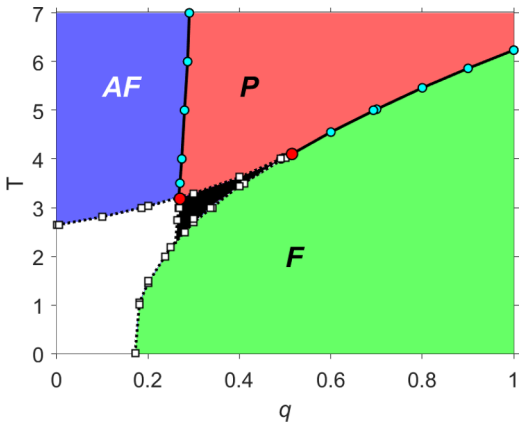

FIG. 4. Phase diagram of the Ising model with competition between Glauber and Kawasaki dynamics on a network with a power-law degree distribution. This diagram presents regions with different colors and denotes the stable phases, AF (purple in the upper left corner), F (green in the lower right corner), P (red in the upper right corner), and the metastable phases, AF or F (white), F or P (black). The cyan (light gray) circles indicate second-order phase transition points and the white squares indicate first-order phase transition points. The red (dark gray) points represent the tricritical points. Dotted and straight lines are only guides for the eyes, and the error bars are smaller than the symbol sizes.

and F phases. If the external parameters in the simulation are initialized with values from the black region, then we find the P phase in this region. However, if the parameter values at the beginning of the simulation are in the green region of the diagram, then the black region refers to an F phase.

In Fig. 3(b), since the initial state of the spins is random and the parameters are swept from highest to lowest value, at low values of q, even though it is a dynamics that conserves the order parameter, such as the Kawasaki dynamics prevailing in the system, we always find the AF phase. Increasing q, we found a first-order phase transition between the AF and F ordered phases. From these points, at low values of temperature, we only have the presence of the F phase since the system is simulated in contact with a heat bath at temperature T, where the one-spin-flip dynamics are prominent for high values of q. In this diagram, the metastable states of the first-order phase transitions in the white and black regions are also evident, along with the self-organization phenomenon mentioned in the description of Fig. 2(a), which can also be seen in all diagrams of Figs. 2 and 3.

Using the conditional phase diagrams from Figs. 2 and 3, we can produce a complete phase diagram of the system that includes all points and regions of metastability: the white region, which represents instability between the AF and F phases, and the black region, which represents instability between the F and P phases. This complete phase diagram is presented in Fig. 4 and contains all the points obtained in constructing the conditional phase diagrams.

C. Second-order phase transitions

This subsection aims to present the critical behavior observed in the second-order phase transitions as can be seen in the conditional phase diagrams of Figs. 2 and 3, and the complete phase diagram of Fig. 4. The continuous variation of the order parameter during the transition from an ordered phase to the higher symmetry disordered phase can be identified by analyzing the crossing of the Binder cumulant curves at the phase transition point [24,25]. In our system, the Ising model on the complex network with competing dynamics exhibits two regions in the phase diagram, of T versus q, with second-order phase transitions.

The first region is observed at low values of q and high of T, in the transition from the AF to the P phase as q increases. In this part of the diagram, there is a high external energy flow into the system. Therefore, whereas the dynamics responsible for this energy flow favors the state of higher energy in the system, the AF phase is expected. The AF phase is observed only at high values of T in a second-order phase transition. This occurs because at high T, the only possible steady state in the Glauber dynamics is the disordered phase, P. Thus, there is no competition between two ordered phases, which is one of the main reasons for observing first-order phase transitions in the system, allowing the system to self-organize into the AF phase for low values of q.

The second region where we found second-order phase transitions in the diagrams of Figs. 2–4 are the ones with high values of q. In this case, the dominant dynamics in the system simulate the contact with the heat bath through the one-spin flip mechanism. This dynamics does not conserve the order parameter. Therefore, given favorable conditions, i.e., low temperatures, we will always find the state of lower energy, the F phase, independently of the initial state of the system. This characteristic of the dynamics in the system prevents the existence of metastable states, and we can observe continuous phase transitions between the F to P phases.

In Fig. 5, the Binder cumulant curves for the two types of second-order phase transitions observed are presented. In Fig. 5(a), the crossing of the curves indicates the transition point between AF to P phase as a function of q and for a fixed value of $T = 5.0$. At this same temperature, further increasing q, is observed transitions from the P to F phases, as indicated by the crossing of the Binder cumulant curves in Fig. 5(b). Transitioning from the ordered AF phase to the disordered P phase, and from this disordered phase back to an ordered phase, the F phase, it characterizes the phenomenon of self-organization in our nonequilibrium system.

Another property that we can obtain from the second-order phase transitions is the universality class of the system. This universality class can be identified through critical exponents, which they were obtained here through scale relations in Eqs. (12), (13), and (14). Using these scale relations, there are two main methods to obtain the exponents of the system.

The first method can be seen in Fig. 6, where we have utilized the fact that scale relations are valid in the vicinity of the critical point. By collecting data on thermodynamic quantities at the phase transition for different lattice sizes, the slope of the linear fit of these points on a graph with axes in logarithmic scale returns the ratios between the critical exponents. Using the scale relation of Eq. (12), the points of magnetization at q_c as a function of lattice sizes yield the ratio β/ν, as indicated by the linear fit of the black points in Fig. 6. Similarly, using the relation of Eq. (13), the

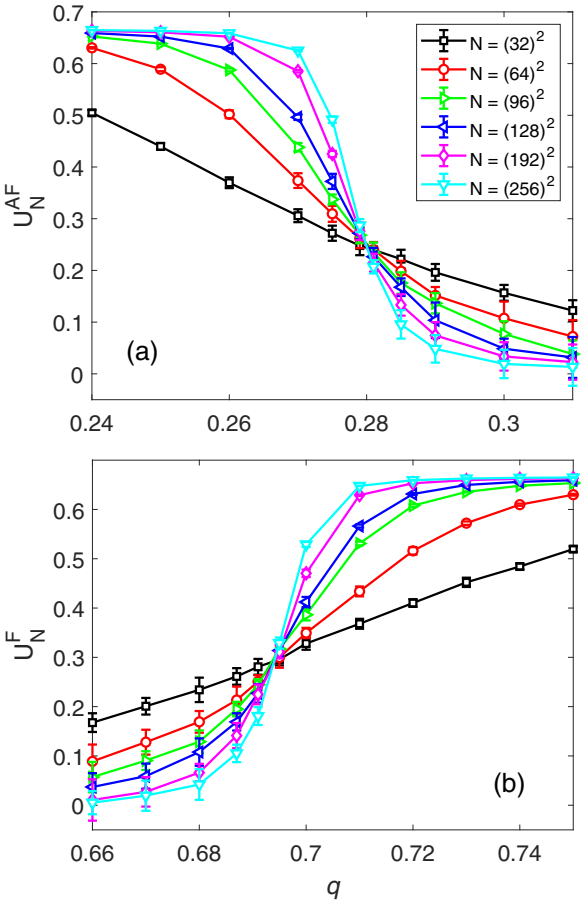

FIG. 5. Binder cumulants U_N^{AF} (a) and U_N^F (b) as a function of the competition parameter q, and for a fixed value of $T = 5.0$. The crossing point for different network sizes N (see in the figure) indicates the second-order phase transition point in $q_c = 0.28 \pm 0.005$ (a) and $q_c = 0.694 \pm 0.005$ (b).

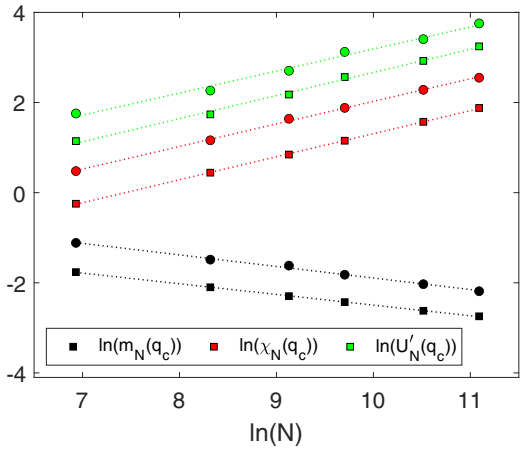

FIG. 6. Linear fit of the thermodynamic quantities at the critical point as a function of the network size N, and for a fixed value of $T = 5.0$. The square symbols represent the values of the m_N^{AF}, χ_N^{AF}, and U_N^{AF}, already the circle symbols indicate the values of the m_N^F, χ_N^F, and U_N^F. The results are well-fitted by dashed straight lines. The error bars are smaller than the symbol sizes.

susceptibility points show us the ratio γ/ν, while with Eq. (14), utilizing data from the derivative of the Binder cumulant, we obtain information about the exponent related to the correlation length, $1/\nu$. The linear fit for the ratios γ/ν and $1/\nu$ can be seen respectively in the red (dark gray) and green (light gray) points in Fig. 6. Additionally, in this figure, the square points indicate the thermodynamic quantities at the transition between the AF to P phases, while circle points denote the quantities at the transition between the P to F phases. In these two transitions, equivalent critical exponents are obtained for $T = 5.0$. At the AF to P phase transition, therefore, we found $(\beta/\nu)_{AF} = 0.24 \pm 0.01$, $(\gamma/\nu)_{AF} = 0.51 \pm 0.02$, and $(1/\nu)_{AF} = 0.51 \pm 0.09$, while at the P to F phase transition we have obtained $(\beta/\nu)_F = 0.26 \pm 0.06$, $(\gamma/\nu)_F = 0.50 \pm 0.06$, and $(1/\nu)_F = 0.49 \pm 0.09$.

Another method that we can employ to find the critical exponents of the system is data collapse. In this method, the goal is to find the scaling function contained in the scaling relations by collapsing the curves of thermodynamic quantities with different lattice sizes. To achieve this, isolating the scaling function from the scaling relations, i.e., plotting $m_N N^{\beta/\nu}$ against $\epsilon N^{1/\nu}$ for magnetization curves, we have adjusted the critical exponents until we obtained a single curve with the different lattice sizes. When this occurs, the exponents used in this data collapse are the critical exponents of the system, since the scaling function is only obtained in the vicinity of the critical point and if the correct critical exponents of the system are used. In Fig. 7(a), we have presented the data collapse for the magnetization curves, m_N^{AF} and m_N^F, while in Fig. 7(b), the data collapse for the susceptibility curves in the two types of transitions can be seen. These plots were made with logarithmic scales axes as this also allows us to identify the asymptotic behavior, far from q_c, of the scaling functions through the slope Θ presented in Figs. 7(a) and 7(b). Fixed at $T = 5.0$, for the collapse of curves at the AF transition, we used $(\beta/\nu)_{AF} = 0.25$, $(\gamma/\nu)_{AF} = 0.50$, $(1/\nu)_{AF} = 0.50$, e $q_c = 0.28 \pm 0.005$, and at the F transition, we have used the exponents $(\beta/\nu)_F = 0.23$, $(\gamma/\nu)_F = 0.52$, e $(1/\nu)_F = 0.50$, along with the phase transition point $q_c = 0.694 \pm 0.005$.

In both methods used for calculating the critical exponents, we obtained equivalent results. We also calculated the critical exponents for other temperature values and verified that these are also in accordance with those obtained from the mean-field approximation, since $\beta = 0.5$, $\gamma = 1.0$, e $\nu = 2.0$. These exponents are expected because we are dealing with the Ising model on a complex network where the second and fourth moments of the degree distribution are convergent [26]. With this result, we have further evidence that the Ising model belongs to the same universality class both in thermodynamic equilibrium and out of it [21].

D. First-order phase transitions

As mentioned in the description of the phase diagrams in Figs. 2–4, we found first-order transitions at low values of q. In this part of the diagrams, when we decrease q, we increase the external energy flow into the system. In this case, the Kawasaki dynamics tend to govern the system. As a dynamic that conserves the order parameter, it depends on initial conditions or complementary dynamics to reach specific steady

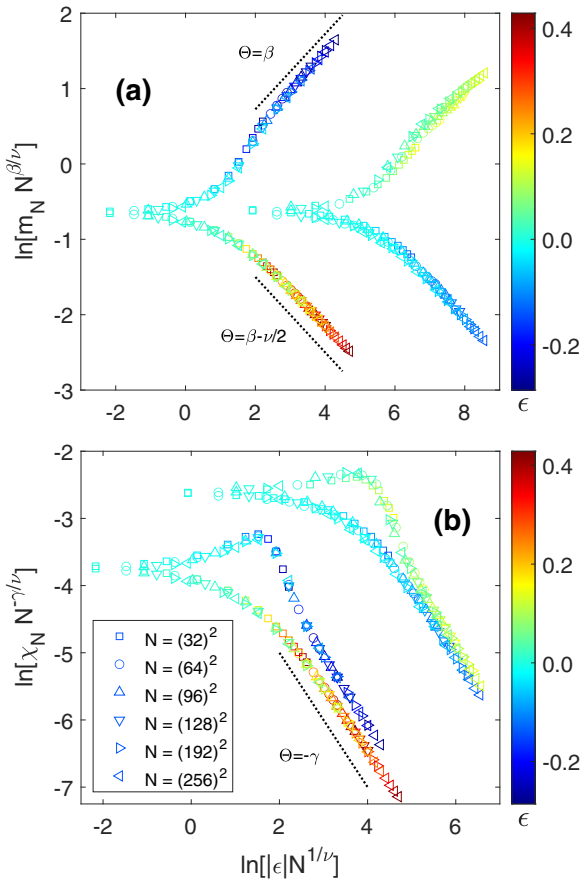

FIG. 7. Data collapse of the magnetizations (a) and susceptibilities (b) for different network sizes N, as indicated in the figure, and for a fixed value of $T = 5.0$. The curves of m_N^{AF} and χ_N^{AF} can be seen in the right side of the figures, and for m_N^F and χ_N^F the collapsed curves are in the left side of the figures. The data collapse validates our estimates for the critical parameters β/ν, γ/ν, $1/\nu$, and q_c. The error bars are smaller than the symbol sizes.

states. If we only have the Kawasaki dynamics acting on the system ($q = 0$), as it is predefined to favor the higher-energy state, and if the initial state of the system is F, then it will not be altered because the dynamics do not change the spin states. Additionally, if the initial state of the system is P, then the system evolves to the AF state, whereas this is the higher-energy state and the initial spin states do not need to be altered, only exchanged with each other. Now, if the system has an initial AF state, then it remains unchanged. However, if we have a nonzero probability of the one-spin flip dynamics acting on the system ($q \neq 0$), as it is strongly dependent on temperature and favors the lower-energy state of the system, at high values of T, then the spin states are altered to have the disordered state P as the steady state. Yet, if q remains small, at these temperature values, then the state of the system can be organized into the AF phase because the Kawasaki dynamics still dominates the system. This phase is observed in all diagrams of Figs. 2–4 at second-order phase transitions.

For low values of T and $q \neq 0$, we have two ordered state possibilities for the system. This is because, from the Glauber dynamics, the steady state is the F phase, while from the Kawasaki dynamics, we expect the AF phase. In this case, the

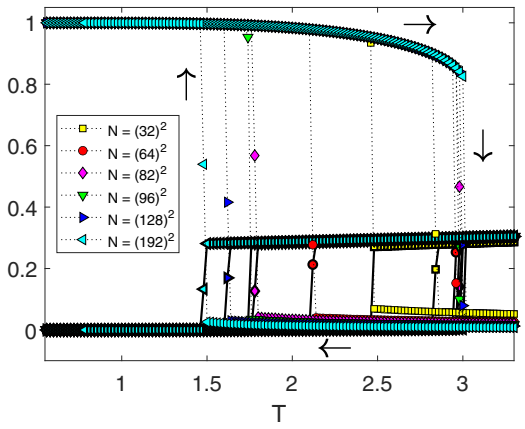

FIG. 8. Behavior of the magnetization m_N^F (dotted lines) and m_N^{AF} (solid bold lines) as a function of T, and for different network sizes N, as indicated in the figure. Here, we used the fixed value of $q = 0.2$. These hysteresis-type curves were obtained with the ordered F initial state of the system, we start from the smallest to the largest value of T, and then in the opposite direction, as indicated by the arrows in the figure. The error bars are smaller than the symbol sizes.

initial state of the system makes a total difference, because starting from the initial F state [see Fig. 2(a)], even with the Kawasaki dynamics as the most dominant in the system, we do not find any other phase than F, which prevails for all values of q. However, if we have a disordered initial state [see Figs. 3(a) and 3(b)] or we start from an ordered state that becomes disordered by the Glauber dynamics due to high temperatures [see Fig. 2(b)], then the system evolves into the ordered AF state when the Kawasaki dynamics dominates. However, in this low-temperature regime, there is also competition between ordered phases, as there are favorable conditions for the F phase of the Glauber dynamics. So, if we decrease the external energy flow and the system is dominated by the heat bath, i.e., increasing q, then an abrupt transition from the AF to F phases is observed. It is in this transition between the ordered phases that we find the majority of the first-order transitions in the system. This transition between ordered phases can also be observed by changing the temperature of the system, because at low values of q and initial F state, increasing T, transitions to AF phase is observed.

Due to the metastable states close to first-order phase transitions, one way to identify these transitions is by examining the dependence of the transition point on the system size. Another result of this instability is the possibility of obtaining hysteresislike curves by changing the direction of parameter sweeping in first-order phase transitions. One of the most interesting points to observe these instabilities is $q = 0.2$ because it passes through all ordered phases and regions where both the ordered F phase and the ordered AF phase can exist. In Fig. 8, for the ordered initial state in the system, we present the plot of m_N^{AF} and m_N^F at $q = 0.2$ as a function of T, varying from the lowest to the highest temperature, and then reversing, varying from the highest to the lowest temperature. Comparing these magnetizations with the phases obtained in the diagrams of Fig. 2, we can see that the approximate point where m_N^F tends to zero is precisely on the transition line from the F to AF phase observed in the diagram of Fig. 2(a). As we

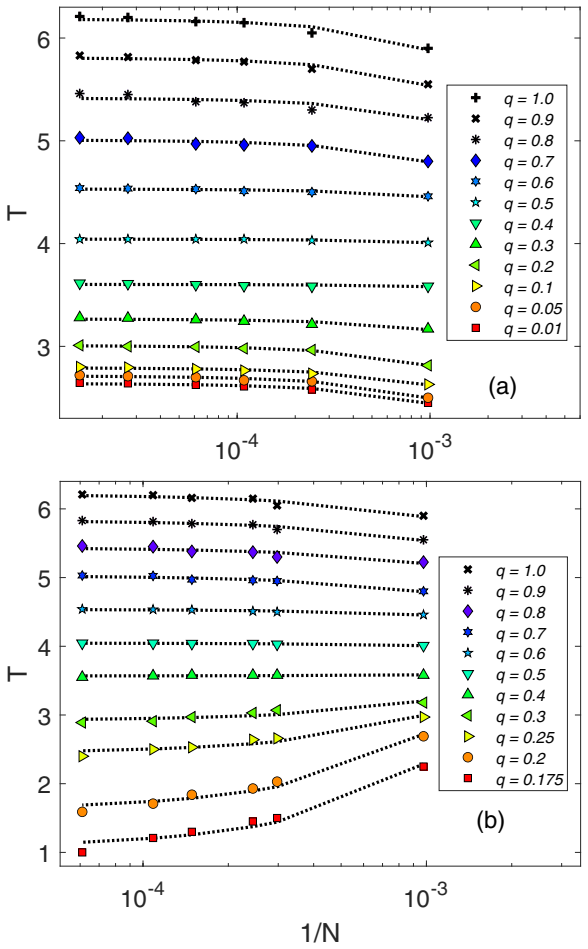

FIG. 9. Linear adjustment of the temperature where we have the susceptibility peak, as a function of the inverse of the network size N, to estimate the critical point in the system. In the adjustments in panel (a), we have networks with sizes ranging from $N = (32)^2$ to $N = (256)^2$, and in panel (b), networks with sizes ranging from $N = (32)^2$ to $N = (128)^2$. These were used to find the critical points in Figs. 2(a) and 2(b), respectively. Here the x axis is on a logarithmic scale just to better visualize the points, and the error bars are smaller than the symbol sizes.

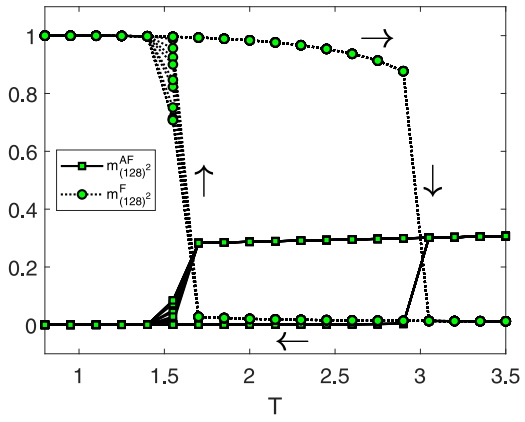

FIG. 10. Behavior of the magnetizations as a function of T of the system for network size $N = (128)^2$ and $q = 0.2$. We performed 10 cycles of variation of T, where the initial state of the system was with all spins in the same state. The error bars are smaller than the symbol sizes.

decrease the temperature, we already have a nonzero value for m_N^{AF}, transitioning from the AF to F phase in the vicinity of the transition point in the diagram of Fig. 2(b).

Owing to system-size dependence, we cannot use the crossing of the fourth-order Binder cumulant curves to obtain the first-order transition points of the system. However, we can use the linear behavior of the peaks of the magnetic susceptibility for different lattice sizes. In this case, we extrapolated the value of the critical point to an infinite-sized lattice, assuming that $T_c(\chi_N^{\max}) = N^{-1}\Delta + T_c(\chi_{N\to\infty}^{\max})$, where $T_c(\chi_N^{\max})$ is the pseudo-critical point for each lattice size and $T_c(\chi_{N\to\infty}^{\max})$ is the extrapolation of the critical point for infinite lattices. Thus, we can fit $T_c(\chi_N^{\max})$ as a function of N^{-1} to obtain an estimate for $T_c(\chi_{N\to\infty}^{\max})$ with the linear coefficient of this fit. Examples of these fits for different values of q and for both first-order and second-order phase transitions can be seen in Fig. 9, where we have placed the N^{-1} axis on a logarithmic scale for better visualization of the points for the different lattice sizes after estimating the phase transition points. In Fig. 9(a), we have the adjustments for the points used in Fig. 2(a), where we sweep the external parameters from the lowest to the highest value, while in Fig. 9(b), the adjustments correspond to the points used in Fig. 2(b), where we sweep the external parameters from the highest to the lowest value.

As seen in Fig. 8, the hysteresislike curves become even more unstable when dealing with regions in the phase diagram where two types of phases can coexist. Another way to observe this characteristic is by performing multiple loops of the external parameter, in this case T, for $q = 0.2$, thus creating several hysteresis curves, as shown in Fig. 10. In this case, we have a single path when increasing T, but when we reverse the way, decreasing T, in this region where both phase F and phase AF can exist, we observed variations regarding the point where the transition between the ordered phases occurs.

When we decrease the external energy flux into the system, we reduce the main reason for the existence of first-order phase transitions, i.e., the coexistence between two ordered phases, as the prevailing dynamics in the system depends only on temperature and not on the initial state of the system or auxiliary dynamics. The reduction in system instability until it reaches the second-order phase transition as q increases can be observed in Fig. 11: for the ferromagnetic magnetization curves in Fig. 11(a), Binder cumulant in Fig. 11(b), and magnetic susceptibility in Fig. 11(c). In this figure, the hysteresis curves were constructed somewhat differently from those in Figs. 8 and 10. The curves with square points represent the results of the system with an ordered initial state, where all sites have the same spin value, while the points of the curves with circles represent a system with a random initial state. Additionally, the dashed curves indicate that T was swept from higher to lower values, while the solid curves indicate that the temperature was swept from lower to higher values.

Another interesting point, that we can observe in Fig. 11 and in the phase diagrams of Figs. 2 and 3, is the existence of absorbing states which can be found at $q \lesssim 0.172$. In the case of $q = 0.1$, Fig. 11 provides an example of how this absorbing state arises, i.e., starting from the ordered state and increasing the temperature, looking at m_N^F, we have a transition from

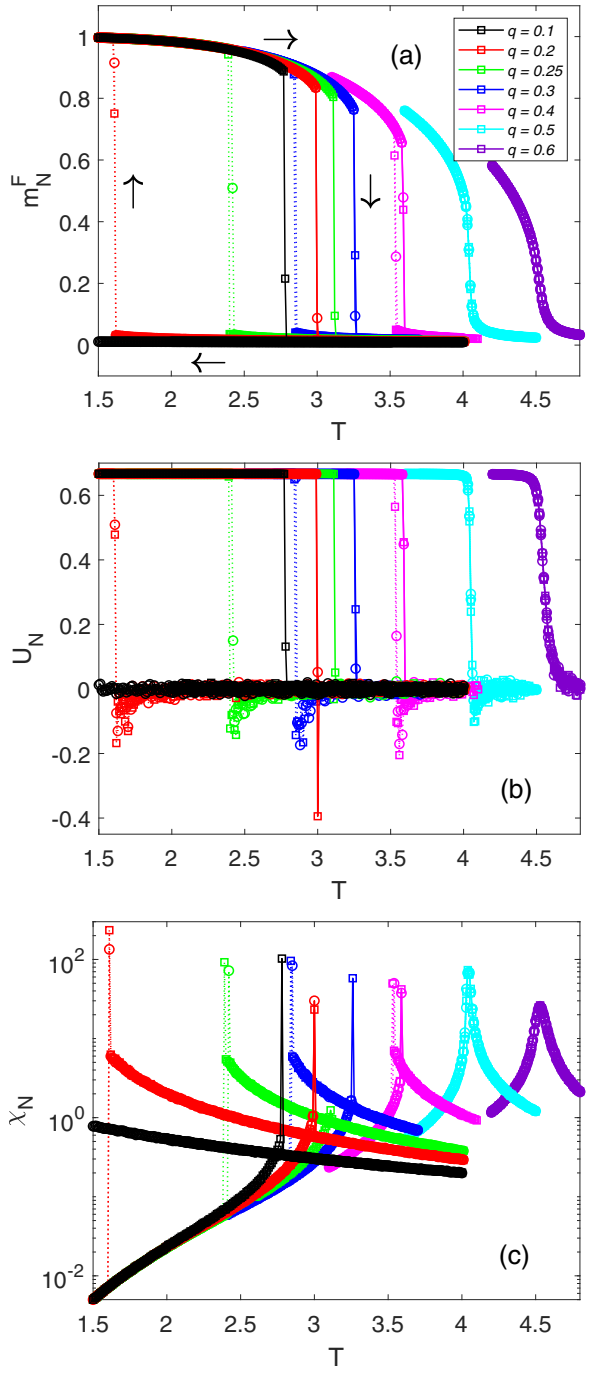

FIG. 11. Behavior of the thermodynamic quantities of the system m_N^F (a), U_N (b), and χ_N (c). Here are presented curves for different values of q (from the left side $q = 0.1$ to the right side $q = 0.6$) as a function of T, and network size $N = (128)^2$. The solid curves denote the sweep of T from the smallest to the largest value, while the dotted curves denote the sweep of T from the largest to the smallest value. The curves with square points indicate that the system had an initial state with a ordered F state, while in the curves with circular points the initial state of the system was disordered. The error bars are smaller than the symbol sizes.

F to P phase, but when we return in the opposite direction by decreasing the temperature, we have not reached the F phase again. However, if we start from a disordered initial state, characteristic of phase P, then we never reach phase F. Another example of this absorbing state, which can be identified at $q \lesssim 0.172$, is not shown here but can be analyzed in Figs. 2 and 3. Looking at m_N^{AF}, if initially all spins in the system are in the same state, then increasing the temperature transitions from phase P to phase AF is observed. But, if we reverse the path by decreasing the temperature, then we do not reach phase P again, only observing AF phase. Starting from a random initial state and still considering m_N^{AF}, we always found phase AF as the steady state. This indicates that for $q \lesssim 0.172$, we find the absorbing state by increasing the temperature, during the transition from the F phase to the AF phase. Once this AF phase is reached, we cannot exit it by decreasing the temperature. This characterizes the absorbing states and can be further verified in the phase diagrams of Figs. 2–4 for $q \lesssim 0.172$.

In the phase diagrams of Figs. 2–4, we have found both first- and second-order phase transitions, and the point where one type of transition starts and the other ends, where we can identify as the tricritical point. We do not have a very precise technique to define the tricritical point, but we can analyze some evidence that characterizes these types of phase transitions (first- and second-order) and estimate the value of this point. The most common way of distinguishing these two types of phase transitions is the continuity of the order parameter. For low values of q, we have a discontinuity of the order parameter in the first-order phase transition, while the continuous phase transition for high values of q characterizes the second-order phase transitions (see Fig. 11). In addition to the discontinuity in first-order phase transitions, we also have evidence of coexistence between the ordered and the disordered phases, which can be verified with the distribution of the order parameter in the vicinity of the critical point. Therefore, from Monte Carlo simulations, even if we apparently cannot observe the discontinuity of the order parameter, if we analyze the distribution of this parameter in the vicinity of the critical point and observe the coexistence of phases, then we can identify this as a first-order phase transition.

In Fig. 12(a), we display the distributions of m_N^F, $\rho(m_N^F)$, for some values of q in the vicinity of the transition point. We can see $\rho(m_N^F)$ on the left side before T_c and $\rho(m_N^F)$ on the right side after T_c. Before T_c, we can observe two peaks representing the symmetric values of the order parameter, $\pm m_N^F$. After T_c, we have only one peak, representing only the disordered phase, where $m_N^F = 0$. For low values of q in Fig. 12(a) and at the phase transition, we can observe three peaks, indicating the coexistence of ordered and disordered phases, characteristic of a first-order phase transition. When we increase the values of q, we can not distinguish the peaks corresponding to the coexistence phases, indicating that we have a second-order phase transition. For instance, based on these distributions, we have estimated the tricritical point of the system given by $q_t = 0.515 \pm 0.01$ for $T = 4.10$. Another tricritical point present in the phase diagrams of Figs. 2 and 3 is related to the transitions from the AF to F phase, and it was also estimated by this method, where we obtained $T_t = 3.18 \pm 0.02$ for $q = 0.27$.

We can also observe the values of the Binder cumulant at the first-order phase transition. For this, with the same values of q as in the distributions of Fig. 12(a), we

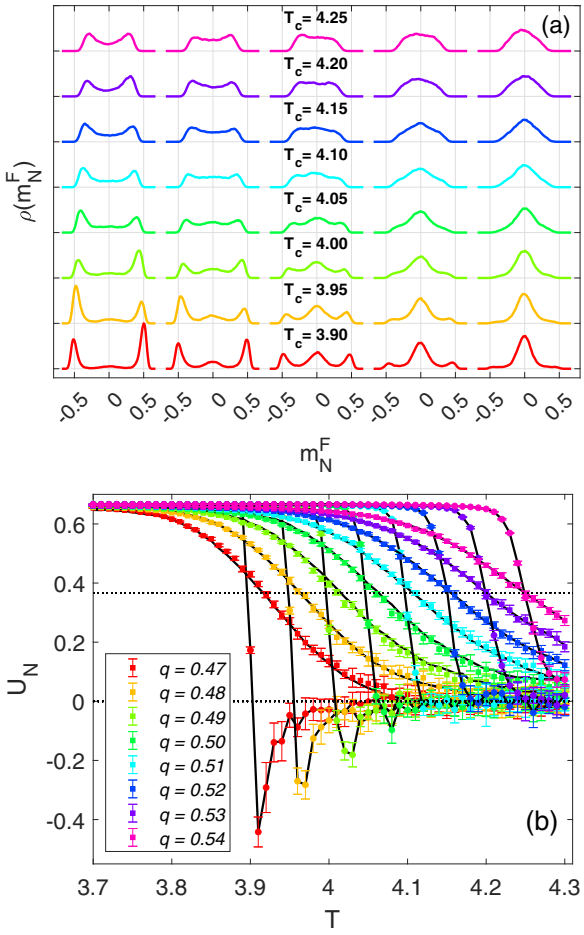

FIG. 12. (a) The distribution $\rho(m_N^F)$ is presented for five values of T around T_c ($T = T_c - 0.01$, $T = T_c - 0.005$, $T = T_c$, $T = T_c + 0.005$, $T = T_c + 0.01$, respectively), and values of q near the tricritical point. Here, we used $N = (128)^2$. (b) Binder cumulant U_N for m_N^F with two network sizes $L = (32)^2$ (square symbols) and $L = (128)^2$ (circle symbols). The horizontal dashed lines are for $U_N = 0$ and the crossing of the curves for $q = 0.54$ at $U_N = 0.367$. The colors of the curves in panel (a) (from $q = 0.47$ a the bottom to $q = 0.57$ at the top) refer to the q values presented in panel (b) (from $q = 0.47$ on the left side to $q = 0.57$ at the right side).

present the curves for two different network sizes for the Binder cumulant in Fig. 12(b). With these curves, we can see that the Ising model on a complex network with competitive dynamics and in the first-order phase transitions, also presents negative values of the Binder cumulant. The dashed lines in Fig. 12(b) indicate references at $U_N = 0$, and the point where the curves cross for $q = 0.54$, $U_N = 0.367$. This last reference line indicates that the crossing of the U_N curves changes their values, and this remains even in the second-order phase transitions, and when $q = 1.0$ the crossing is at $U_N = 0.26$.

V. CONCLUSIONS

We have employed Monte Carlo simulations to investigate the Ising model on a network with power-law degree distribution, subject to two competing dynamics. Considering the ferromagnetic coupling between spins, with probability q, the system is governed by Glauber dynamics, favoring the lowest energy state, while with probability $1 - q$, the Kawasaki dynamics evolves the system toward the highest energy state. Given that Kawasaki dynamics conserves the order parameter, we built the phase diagrams T versus q with different initial states in the simulations. The topology of theses diagrams revealed regions with both first- and second-order phase transitions, leading to the discovery of tricritical points at coordinates ($q = 0.27$, $T_t = 3.18 \pm 0.02$) in the AF to F transition, and ($q_t = 0.515 \pm 0.01$, $T = 4.1$) in the F to P transition. The tricritical points in the F to P transition have already been verified in systems dealing with these competing dynamics [8,22]. However, in the present work, a tricritical point is also observed in the AF to F transition, which is a result of the high average coordination number of the network used. In regions of second-order phase transitions, just like in other nonequilibrium systems on complex networks [18,19], we find critical exponents from mean-field approximation, $\nu = 2$, $\gamma = 1$ and $\beta = 0.5$, predicted for systems in thermodynamic equilibrium with networks where the second and fourth moments of the degree distribution converge [26]. However, unlike systems employing dynamics that do not conserve the order parameter [18,19], the phase diagrams presented here exhibit first-order phase transitions. This region, characterized by a discontinuity in the order parameter, altered the phase diagram topology depending on the initial conditions of the system and arises due to the competition between AF and F ordered phases. Absorbing states have been identified in the system for below $q = 0.172$, during the transition from the F phase at low temperatures to the AF phase at high temperatures, remaining in this phase even when the temperature is decreased again. Finally, for $3.18 \leqslant T \leqslant 6.235$, we also observed the phenomenon of self-organization, which is common in systems with competing dynamics that favor different ordered states [3–5,8,18,19,22]. Here, at low q values, the system exhibits the AF phase, transitioning to the P phase as q increases, and further transitioning to an ordered phase, F phase, for higher q.

ACKNOWLEDGMENTS

This work has been supported by the Conselho Nacional de Desenvolvimento Científico e Tecnológico (CNPq), Brazil (Process No. 140141/2024-3).

[1] J. W. Gibbs, *Elementary Principles in Statistic Mechanics* (Yale Universality Press, New Haven, CT, 1902).
[2] J. M. Gonzalez-Miranda, P. L. Garido, J. Marro, and J. L. Lebowitz, Phys. Rev. Lett. **59**, 1934 (1987).
[3] T. Tomé and M. J. de Oliveira, Phys. Rev. A **40**, 6643 (1989).
[4] B. C. S. Grandi and W. Figueiredo, Phys. Rev. B **50**, 12595 (1994).

[5] T. Tomé, M. J. de Oliveira, and M. A. Santos, J. Phys. A: Math. Gen. **24**, 3677 (1991).
[6] R. J. Glauber, J. Math. Phys. **4**, 294 (1963).
[7] K. Kawasaki, Phys. Rev. **145**, 224 (1966).
[8] A. Szolnoki, Phys. Rev. E **62**, 7466 (2000).
[9] D. J. Watts and S. H. Strogatz, Nature (London) **393**, 440 (1998).
[10] M. E. J. Newman and D. J. Watts, Phys. Rev. E **60**, 7332 (1999).
[11] S. Milgram, Psychol. Today **2**, 60 (1967).
[12] A.-L. Barabási and R. Albert, Science **286**, 509 (1999).
[13] R. Albert and A.-L. Barabási, Rev. Modern Phys. **74**, 47 (2002).
[14] A. L. M. Vilela, B. J. Zubillaga, C. Wang, M. Wang, R. Du, and H. E. Stanley, Sci. Rep. **10**, 8255 (2020).
[15] B. J. Zubillaga, A. L. M. Vilela, M. Wang, R. Du, G. Dong, and H. E. Stanley, Sci. Rep. **12**, 282 (2022).
[16] D. S. M. Alencar, T. F. A. Alves, R. S. Ferreira, F. W. S. Lima, G. A. Alves, and A. Macedo-Filho, Physica A **626**, 129102 (2023).
[17] J. Wang, W. Liu, F. Wang, Z. Li, and K. Xiong, Eur. Phys. J. B **97**, 22 (2024).
[18] R. A. Dumer and M. Godoy, Phys. Rev. E **107**, 044115 (2023).
[19] R. A. Dumer and M. Godoy, Physica A **626**, 129111 (2023).
[20] R. A. Dumer and M. Godoy, Eur. Phys. J. B **95**, 159 (2022).
[21] R. A. Dumer and M. Godoy, Physica A **621**, 128795 (2023).
[22] W. Liu, Z. Yan, and G. Zhou, Open Phys. **17**, 1 (2019).
[23] H. Hong, M. Ha, and H. Park, Phys. Rev. Lett. **98**, 258701 (2007).
[24] S.-H. Tsai and S. R. Salinas, Braz. J. Phys. **28**, 58 (1998).
[25] L. Böttcher and H. J. Herrmann, *Computational Statistical Physics*, 1st ed. (Cambridge University Press, New York, NY, 2021).
[26] A. V. Goltsev, S. N. Dorogovtsev, and J. F. F. Mendes, Phys. Rev. E **67**, 026123 (2003).